

Coherent beam combining of a narrow-linewidth long-pulse Er³⁺-doped multicore fiber amplifier

F. PREVOST,^{1,*} L. LOMBARD,^{1,*} J. PRIMOT,¹ L. P. RAMIREZ,² L. BIGOT,³ G. BOUWMANS,³ AND M. HANNA²

¹Onera, The French Aerospace Lab, Palaiseau, France

²Laboratoire Charles Fabry, Institut d'Optique Graduate School, CNRS, Université Paris-Saclay, 91127 Palaiseau cedex, France

³Physique des Lasers Atomes et Molécules, IRCICA-Institut de Recherche sur les Composants Logiciels et Matériels pour l'Information et la Communication Avancée, CNRS, UMR 8523,F-59000,France

*Laurent.Lombard@onera.fr

Abstract: Active phase locking of a multicore erbium-doped fiber amplifier is demonstrated for 180 ns narrow-linewidth pulses at 1545 nm. A spatial light modulator is used at the input of the amplifier to control the optical phase of 7 beams injected in the hexagonally-arranged cores, ensuring efficient combining through a SPGD algorithm. At the output, combining is performed using a diffractive optical element. This experiment establishes multicore amplifiers as a promising way to scale the energy of Brillouin-limited pulsed amplifiers for LIDAR applications. We also present a simple lensless technique to measure phase shifts between pairs of adjacent channels that could be implemented in future active coherent combining systems.

© 2017 Optical Society of America

OCIS codes: (140.3298) Laser beam combining; (140.3500) Lasers, erbium; (060.2320) Fiber optics amplifiers and oscillators; (140.3538) Lasers, pulsed.

References and links

1. A. Dolfi-Bouteyre, G. Canat, M. Valla, B. Augere, C. Besson, D. Goular, L. Lombard, J.-P. Cariou, A. Durecu, D. Fleury, L. Brictieux, S. Brousmiche, S. Lugan, and B. Macq, "Pulsed 1.5- μm LIDAR for axial aircraft wake vortex detection based on high-brightness large-core fiber amplifier," *IEEE J. Sel. Top. Quantum Electron.* **15**(2), 441–450 (2009).
2. W. Shi, E. B. Petersen, Z. Yao, D. T. Nguyen, J. Zong, M. A. Stephen, A. Chavez-Pirson, and N. Peyghambarian, "Kilowatt-level stimulated-Brillouin-scattering-threshold monolithic transform-limited 100 ns pulsed fiber laser at 1530 nm," *Opt. Lett.* **35**(14), 2418–2420 (2010).
3. A. Brignon, *Coherent Laser Beam Combining* (John Wiley & Sons, 2013)
4. L. Lombard, A. Azarian, K. Cadoret, P. Bourdon, D. Goular, G. Canat, V. Jolivet, Y. Jaouën, and O. Vasseur, "Coherent beam combination of narrow-linewidth 1.5 μm fiber amplifiers in a long-pulse regime," *Opt. Lett.* **36**(4), 523–525 (2011).
5. M. Hanna, F. Guichard, Y. Zaouter, D. N. Papadopoulos, F. Druon, and P. Georges, "Coherent combination of ultrafast fiber amplifiers," *J. Phys. At. Mol. Opt. Phys.* **49**(6), 062004 (2016).
6. L. P. Ramirez, M. Hanna, G. Bouwmans, H. El Hamzaoui, M. Bouazaoui, D. Labat, K. Delplace, J. Pouysegur, F. Guichard, P. Rigaud, V. Kermène, A. Desfarges-Berthelemot, A. Barthélémy, F. Prévost, L. Lombard, Y. Zaouter, F. Druon, and P. Georges, "Coherent beam combining with an ultrafast multicore Yb-doped fiber amplifier," *Opt. Express* **23**(5), 5406–5416 (2015).
7. P. Rigaud, V. Kermene, G. Bouwmans, L. Bigot, A. Desfarges-Berthelemot, D. Labat, A. Le Rouge, T. Mansuryan, and A. Barthélémy, "Spatially dispersive amplification in a 12-core fiber and femtosecond pulse synthesis by coherent spectral combining," *Opt. Express* **21**(11), 13555–13563 (2013).
8. G. D. Goodno, C.-C. Shih, and J. E. Rothenberg, "Perturbative analysis of coherent combining efficiency with mismatched lasers," *Opt. Express* **18**(24), 25403–25414 (2010).
9. L. Lombard, C. Bellanger, G. Canat, L. Mugnier, F. Cassaing, V. Michau, P. Bourdon, and J. Primot, "Collective synchronization and phase locking of fs fiber amplifiers: Requirements and potential solutions," *Eur. Phys. J. Spec. Top.* **224**(13), 2557–2566 (2015).
10. M. A. Vorontsov, G. W. Carhart, and J. C. Ricklin, "Adaptive phase-distortion correction based on parallel gradient-descent optimization," *Opt. Lett.* **22**(12), 907–909 (1997).
11. J. Le Dortz, M. Antier, J. Bourderionnet, C. Larat, E. Lallier, and A. Heilmann, ihsan fsaifes, L. Daniault, S. Bellanger, C. Simon-Boisson, J.-C. Chanteloup, and A. Brignon, "Coherent beam combining of 19 fibers in

- femtosecond regime,” in Conference on Lasers and Electro-Optics (Optical Society of America, 2016), paper STu1M.1.
12. J. M. Armstrong, M. R. Skokan, M. A. Kinch, and J. D. Luttmer, “HDVIP five-micron pitch HgCdTe focal plane arrays,” *Proc. SPIE* **9070**, 907033 (2014).

1. Introduction

Power scaling of fiber-based laser sources has shown tremendous progress over last decades. However, applications require ever-increasing performances, in various temporal regimes. An example of such application is Doppler LIDAR, where long (~ 100 ns) energetic (~ 100 μ J - 1 mJ) narrow-linewidth pulses are used to probe wind speed [1] in the atmosphere. In this regime, Brillouin scattering limits the peak power at the output of large mode area fiber amplifiers to around 1 kW [2].

Coherent Beam Combining (CBC) is now widely recognized as a way to scale the power and energy of laser sources while retaining the spatial and temporal properties of a single source. This process ideally allows power scaling by a factor equal to the number of amplified beams. CBC has been particularly investigated for fiber amplifiers, since the well-controlled beam quality facilitates its implementation [3]. When operated in pulsed regime, one of the main drawbacks of fiber amplifiers is that the achievable output energy is much lower than that of bulk amplifier, due to enhanced nonlinear effects. CBC has therefore been particularly useful in the context of pulsed fiber amplifiers, e. g. in the nanosecond [4] or femtosecond [5] regimes. The vast majority of demonstrations of CBC has been done with Yb-doped fibers, allowing the highest output powers.

Multicore fibers (MCF) have also attracted attention as a way to provide integration to CBC systems: instead of using separate fibers, amplification can be distributed over several independent cores of a single fiber. The CBC system can use a single element to provide phase control to the beams, such as a spatial light modulator (SLM) [6], or a deformable mirror [7] and a single pump source can also be used. Moreover, since the cores share the same environment, it has been shown that optical phase fluctuations are reduced, allowing the use of a much slower feedback system to control them.

In this Letter, we demonstrate CBC of a 7-core Er-doped fiber amplifier in the eye-safe wavelength region, operated in narrow-linewidth 100 ns pulse regime. Phase control is based on a stochastic parallel gradient descent algorithm controlling a SLM, while beam combining is achieved using a diffractive optical element (DOE), resulting in an excellent output beam quality. We obtain a combining efficiency of 63%, to be compared with the unoptimized DOE theoretical efficiency of 75%. This work is a promising step towards multi-kW peak power systems for Doppler LIDAR applications.

2. The erbium doped multicore fiber

The MCF shown in Fig. 1(a) was custom designed and fabricated using the stack and draw technique. Each Er-doped core is single mode at the signal wavelength of 1545 nm and has a mode field diameter of 15.5 μ m. The index step is measured to be 0.0038, as shown in Fig. 1(b) displaying the index profile of a single core. The corresponding numerical aperture is 0.1. In order to provide a polarization-maintaining behavior for each core, boron rods are inserted to induce a birefringence of 1.6×10^{-4} . The distance between neighbor cores is 85 μ m with 1 μ m of standard deviation.

By coupling light in a single core at the input and observing the output beam, no optical coupling between cores is observed, so that each core behaves as an independent fiber amplifier. No pump clad was included for this proof-of-principle demonstration, implying that the MCF must be core-pumped. Although adding a pump clad would make the fabrication process more difficult, in particular with respect to the accurate control of inter-core distance, it will be considered in future work. The measured absorption of one core is 7 dB at 1480 nm, the pump wavelength, while the peak value of absorption is 15 dB at 1530 nm in 1 m of MCF.

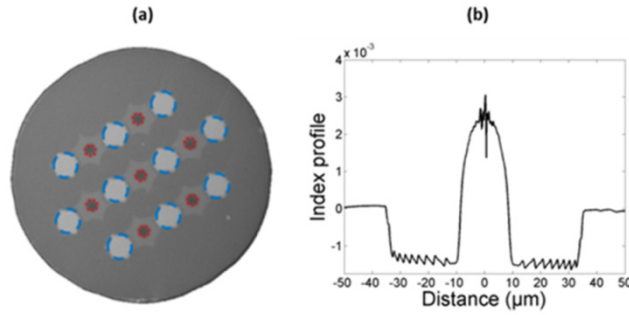


Fig. 1. (a) Picture of the erbium-doped multicore fiber facet. Red circles correspond to erbium-doped cores and blue circles to boron rods for polarization maintaining. (b) Measured index profile of one core of the MCF.

3. Experimental setup

The experimental setup is depicted in Fig. 2, based on the MOPA architecture. The input signal to the MCF is generated by an all-fiber setup: a distributed feedback laser diode generates CW radiation at 1545 nm with a linewidth of 5 MHz, and an acousto-optic modulator is used to shape 178 ns FWHM pulses at 20 kHz repetition rate. This signal is preamplified in two stages (Er³⁺ + / Er³⁺ + -Yb³⁺ +) of standard single mode amplifiers. The preamplified signal beam is collimated and sent to a spatial light modulator (SLM). To prevent optical damage on the SLM display (damage threshold ~2W/cm²), the size of the collimated signal beam is chosen to cover the full active surface of the SLM.

To generate the 7 beams for MCF fiber coupling, the SLM displays a phase map equivalent to the sum of seven maps, each of which represents a grating that diffracts the beam to one core. This allows accurate control of the position of each beam in the fiber input facet plane, and the optical phase of each beam. The phase map displayed on the SLM is the phase term of the complex field described by E:

$$E = \sum_{n=1}^{N_{spots}} \exp \left[2i\pi \frac{(x \cdot x_n + y \cdot y_n)}{\lambda \cdot f} \right] \cdot \exp(i\phi_n) \quad (1)$$

where x_n and y_n are the coordinates of each core, ϕ_n are the optical phases of each spot, λ is the wavelength and f is the focal length used for fiber coupling. Due to the overall diffraction efficiency of the SLM, the coupling efficiency to the MCF is approximately 40%. A dichroic mirror is added between the SLM and the fiber input facet to protect the SLM from residual counter-propagating pump light.

We now focus on the subsystem located at the output facet of the fiber, which serves two purposes: it both acts as the signal combiner and core pumping splitter. The pump light is generated by a 5 W average power Raman effect-based single transverse mode fiber source at 1480 nm wavelength. As previously mentioned, the lack of a pump clad structure implies that the pump beam must be coupled to each core, so that 7 pump beams must be generated. The DOE located at the output of the fiber is used in splitting configuration for that purpose, in a counter-propagating geometry. It is a Damman phase-only grating with 75% diffraction efficiency and power uniformity difference better than 1% between useful orders. The optical pumping system includes lenses that are used to match the pump beam to the fiber cores diameter and pitch.

The separation angle θ of the DOE is given by $\sin(\theta) = m\lambda/p$, where m is the diffraction order and p is the grating period. At the pump wavelength, $\theta_p = 3.16$ mrad, while at the signal wavelength, $\theta_s = 3.30$ mrad. The focal length f that must be used for lens L3 to

focus the pump beam onto the fiber output facet, or to collimate the signal and send it to the DOE, is therefore given by

$$f = d_x / \tan(\theta_{p,s}), \quad (2)$$

where d_x is the inter-core distance. This equation implies that there is a tradeoff between optimal pump coupling and optimal signal combining efficiency, related to imperfect input angles of the signal at the output of the amplifier and into the DOE. In our experiment, this focal length must be equal to 26.9 mm to optimize pump injection. We therefore use an adjustable air-space doublet to precisely control this parameter. As a result, the estimated pump power coupled to each core is 345 mW, taking into account the 92% transmission of the dichroic mirror, the 75% DOE efficiency, and a 70% mode matching to the fiber cores. This pump power results in a gain value of approximately 19 dB.

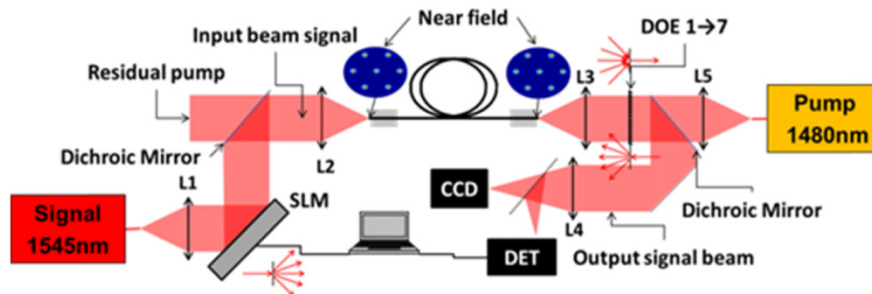


Fig. 2. Experimental setup of the multicore fiber amplifier. Beam shaping of input signal and phase modulation is done by the SLM. The DOE both splits the pump and combines the signal. Active phase-locking is ensured by an SPGD feedback loop.

As shown in Fig. 3, and using the formalism presented in [8], we estimate the loss of signal combining efficiency to be around 12% if optimal pump coupling is chosen. This is the main contributor for the combining efficiency drop, along with the 75% intrinsic diffraction efficiency of the DOE. Additional combining efficiency losses can be expected from the core repartition, the quality of the fiber cleave, the polarization misalignment, the power non-uniformity at multicore fiber output and the beam quality at fiber output. All those losses are low compared to the ~12% chromatic losses and the ~75% diffraction efficiency losses that sum up to ~66% expected overall combining efficiency.

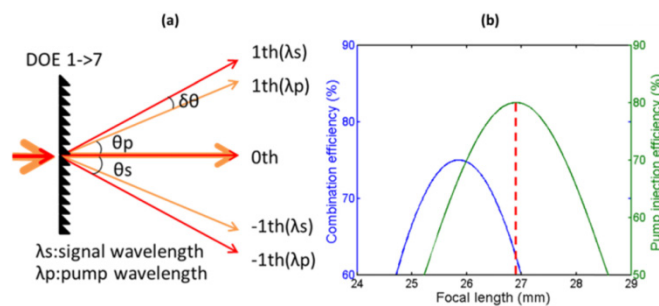


Fig. 3. Left: sketch of dichroism induced by the DOE between signal and pump wavelengths. Right: signal combining efficiency taking into account intrinsic DOE diffraction efficiency (blue) and pump coupling efficiency (green) as a function of focal length of lens L3 on Fig. 2.

4. Phase noise measurement and CBC results

Before implementing the phase-locking feedback loop, we measure phase fluctuations by coupling the seed beam to two adjacent cores of the fiber only, using a setup similar to that

presented in [6]. At the output of the amplifier, we remove the DOE to observe interference fringes in the far field, and two photodiodes are used to measure the in-phase and quadrature components, allowing the measurement of phase fluctuations. The result is shown in Fig. 4(left). The peak-to-peak phase variation is 3 rad during 15 min in 3.7 meters of MCF. This value can be compared to the measurement reported in [6] for two distinct 2 m-long fiber amplifiers, where a peak-to-peak excursion of 180 rad was measured over 50 s. As has been reported previously, the MCF considerably reduces differential environmental phase shifts among cores. Based on this measurement, we can estimate the performance of an ideal first order feedback system in phase-locked operation. The expected residual phase noise is shown in Fig. 4(right) as a function of feedback system bandwidth, and shows that a very slow bandwidth of the order of a fraction of Hertz is sufficient to achieve a residual phase standard deviation of the order of $\lambda/30$ [9].

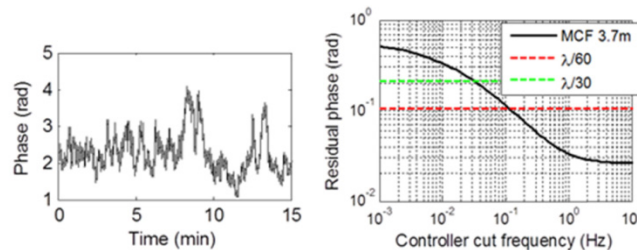


Fig. 4. Left: phase fluctuations measured over 15 min. Right: Simulated residual phase standard deviation as a function of feedback bandwidth.

This feedback loop is implemented through a SPGD algorithm [10]. By applying small random perturbations to the optical phases through the SLM, and measuring their impact, the algorithm continuously optimizes the metric, which in our case is the power contained in the zero-order of the DOE at the output of the system. The bandwidth of a SPGD controller with update rate F is roughly $W = F / 10.N$, with N the number of emitters. In our system, $F = 1.6$ Hz, providing a bandwidth of 0.02 Hz. In closed loop operation, we achieve 63% combining efficiency, defined as the power in the DOE zero-order divided by the total power at the fiber output. Figure 5(a) shows the useful output power as a function of time, and Fig. 5(b) the beam profile at the output of the DOE. Residual uncombined optical power is visible in higher DOE orders. The average output power in the zero-order beam is 378 mW, and the peak power is 105 W. While these numbers are not yet at the state of the art, we strongly believe that optimization of the fiber design and parameters such as doping concentration and pump cladding will allow scaling well beyond the current Brillouin threshold limit for large mode area fibers, around 1 kW.

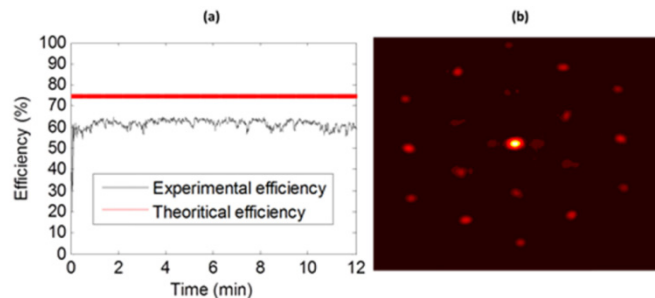


Fig. 5. Left: experimental SPGD metric (corresponding to the power in the DOE zero order) as a function of time. Right: near field beam profile after the DOE in closed loop operation.

The zero-order beam is isolated using a spatial filter in order to proceed with M^2 parameter assessment. The measured value is $M^2 = 1.1 \pm 0.05$ in both transverse directions. Although the input angle to the DOE is non-optimal for the signal as described previously, this does not result in a degradation of the output quality, but rather only in a decrease of the combining efficiency.

5. Intermediate field to measure phase shifts

Finally, residual phase fluctuations between cores in closed loop operation are measured using a novel self-referenced lensless technique that allows us to measure the relative phases between all pairs of adjacent cores. The principle consists in propagating all 7 beams at the output of the MCF without lens to create interference fringes between neighbor cores as illustrated in Fig. 6. To retain phase shift information between two waves, we therefore use the spatial profile in an intermediate plane, where interference patterns between neighbor spots are clearly isolated and distinguishable.

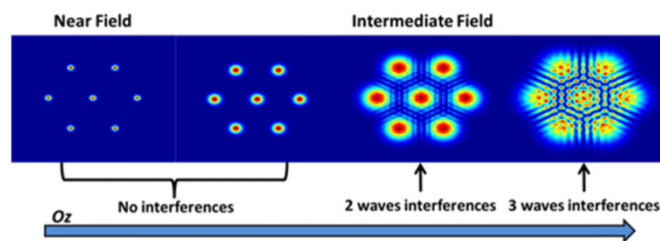


Fig. 6. Theoretical near field and its propagation along the optical axis. In an intermediate field, only adjacent cores interfere in a simple two wave linear fringes pattern. If the phase delay between two cores is changed, the fringe pattern will translate proportionally to the delay. In contrast, the field further away contains interferences between three waves, and the far field (not represented here) is composed of interferences between the seven spots.

The interference pattern is acquired using a CCD camera. As we can see on Fig. 7(a), the fringes position is proportional to the phase shift between the 2 cores that interfere. In our case, 7 cores with hexagonal repartition create twelve areas of interference fringes between peripheral spots and/or the central spot. A simple cut in the middle of each two-wave interference fields allows the measurement of the phase difference evolution between two cores. The time-averaged measured residual phase between all channels is $\lambda/22$ RMS in closed-loop operation, corresponding to 2.5% losses due residual phases according to [8].

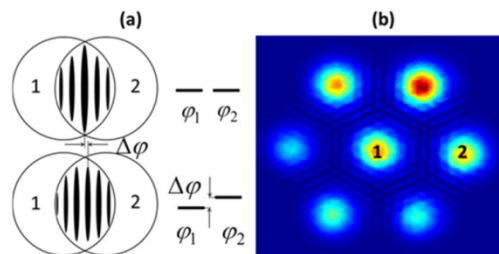


Fig. 7. (a) Schematic representation of fringes shifts between two spots induced by phase fluctuations. (b) Experimental intermediate field, the six areas between the spot number 1 and the peripheral spots correspond to fringes areas used for relative phase shift measurement.

While we used this technique only as a characterizing tool in this experiment, it could advantageously be used as the phase detecting element in the phase feedback loop, allowing deterministic phase control instead of stochastic methods such as SPGD, both for multicore amplifiers and more generally for CBC systems in tiled aperture. Indeed, the relative phase fluctuations to compensate in the feedback loop are acquired at camera refresh rate, whatever

the number of emitters. Moreover, the available light for phase measurement at a fiber amplifier output is usually high even after a 1% beam sampler and the fringe contrast is close to 1. It is thus possible to extract the relative phase fluctuation information with a good signal-to-noise ratio. A least square estimation of the respective phase of all cores is then possible, provided a calibration step.

This method also bears some resemblance with the technique presented in [11]. The main difference is that in our case, a reference wave is not needed and can be made lensless. Indeed, although the results presented here are obtained with an intermediate optical system to adapt the fringe size to a standard camera, it is possible to design a system requiring no optics. For example, in our setup, the distance between the emitters is 80 μm to avoid core coupling. At a distance of 700 μm after the fiber, the beams naturally overlap in the optimal 2 wave interference configuration. We then expect 4 to 5 fringes with a 13 μm period. These patterns can be recorded with e.g. n infrared focal plane array pixel pitch of 5 μm as the HgCdTe sensor presented in [12].

6. Conclusion

In conclusion, we demonstrate for the first time to our knowledge active CBC of a MCF amplifier in the eye-safe wavelength region, in long-pulse operation. This regime is particularly relevant for application to Doppler LIDAR systems where the pulse energy determines the range of the system. The MCF architecture allows power scaling while using single elements for pumping, phase detection, and phase control, providing integration capability to future systems. We present a novel very simple lensless technique to measure phase shift between emitters. This technique can be extrapolated to other setup for example a large number of emitters in square configuration.

Funding

Agence Nationale de la Recherche through the MultiFemto project (ANR 2011 BS09 028 01).